MDPI

Article

Solid-State Synthesis for High-Tetragonality, Small-Particle Barium Titanate

Tianyu Hao [1], Jing Shen [2], Qiaochu Peng [1], Jie Liu [1,*] , Wenbin Hu [1] and Cheng Zhong [1,*]

1   Key Laboratory of Advanced Ceramics and Machining Technology (Ministry of Education), Tianjin Key Laboratory of Composite and Functional Materials, School of Materials Science and Engineering, Tianjin University, Tianjin 300072, China; haotianyu909@163.com (T.H.); qcpeng@tju.edu.cn (Q.P.); wbhu@tju.edu.cn (W.H.)
2   Chongqing Newcent New Materials Co., Ltd., Chongqing 401147, China; shenjing@chinanewcent.com
*   Correspondence: jieliu0109@tju.edu.cn (J.L.); cheng.zhong@tju.edu.cn (C.Z.)

Abstract: This study successfully synthesized high-tetragonality barium titanate ($BaTiO_3$) particles with a small particle size by implementing ball milling in the solid-state synthesis of $BaTiO_3$ and utilizing nanoscale raw materials. This study also addressed the issues of impurities and uneven particle size distribution that could exist in the synthesized $BaTiO_3$ particles. The crystal structure, morphology, and particle size of the synthesized $BaTiO_3$ particles have been meticulously analyzed and discussed through the use of techniques such as X-ray diffraction (XRD), scanning electron microscopy (SEM), and the laser particle size analyzer. $BaTiO_3$ has been successfully synthesized, exhibiting a uniform particle size with an average diameter of 170 nm and a high tetragonality value of 1.01022. This new solid-state synthesis method provided insights to avoid the impact of "size effects" during the process of electronic device miniaturization.

Keywords: barium titanate; solid-state synthesis; tetragonality; size effects; ball milling; mechanochemical method

1. Introduction

Barium titanate ($BaTiO_3$) is a perovskite-type material widely used in multilayer ceramic capacitors (MLCCs) because of its high dielectric constant [1,2]. Among the various structures of $BaTiO_3$, the tetragonal structure has gained significant attention for its distinct features [3–5]. Tetragonal $BaTiO_3$ exhibits a significant property in the form of its tetragonal distortion of the structure cell, commonly referred to as tetragonality (c/a). This property is defined as the ratio of *a* and *c* lattice parameters [6]. Furthermore, tetragonality plays a crucial role in determining the dielectric properties of $BaTiO_3$, as it has been positively correlated with such properties [3]. Thus, high tetragonality is highly desirable for achieving better dielectric properties in $BaTiO_3$, which is particularly beneficial for its application in MLCCs.

In recent years, the miniaturization of MLCCs and electronic devices has become a prominent trend, leading to an increasing demand for electronic components with thin dielectric layers [7,8]. Therefore, the reduction in the particle size in $BaTiO_3$ powders is a general trend. However, studies have indicated that the decrease of $BaTiO_3$ particle size generally results in a reduction in the tetragonality of $BaTiO_3$ particles, which is known as the "size effect" [4]. For example, Uchino et al. [9] observed that a high *c/a* of approximately 1.008 was sustained with the particle size of $BaTiO_3$ being approximately 230 nm, but it decreased to approximately 1.002 at 130 nm. Therefore, it is difficult to prepare $BaTiO_3$ particles that consider both high tetragonality and small particle size.

To this end, various synthesis methods have been made to prepare $BaTiO_3$ with high tetragonality and small particle size. The hydrothermal method produces finely dispersed particles suited for thin dielectric layers [10], but the crystallographic structure may become

cubic and not tetragonal because of the OH group incorporation. The synthesis of $BaTiO_3$ from oxalates often has a complicated procedure. Kita et al. [11] used barium titanyl oxalate as a precursor to prepare $BaTiO_3$ with well-dispersed particle size by the two-step thermal decomposition method. But the decomposition process lasted 5 h and the heat treatment lasted 16 h. Wada et al. [12] also obtained $BaTiO_3$ particles by the two-step thermal decomposition method using $BaTiO(C_2O_4)_2 \cdot 4H_2O$ as the precursors. However, $BaTiO(C_2O_4)_2 \cdot 4H_2O$ was annealed in the O_2 flow in the first step and the precursors were annealed in vacuum in the second step.

The solid-state synthesis method of $BaTiO_3$ involves the calcination of a proportioned mixture of titanium dioxide (TiO_2) and barium carbonate ($BaCO_3$) [13,14]. This traditional method is known for its simplicity, generally resulting in high-tetragonality (*c/a* ratio) $BaTiO_3$ products [15,16]. However, solid-state synthesis methods also have some limitations. The high-temperature calcination process has high energy consumption, and during the calcination process, the particle size distribution of $BaTiO_3$ may be uneven, making it difficult to ensure its morphology. Impurities or incompletely reacted raw materials may also appear. These issues will all affect the electrical properties of $BaTiO_3$ [15,17]. Therefore, some researchers are still committed to innovating and improving solid-state synthesis methods to achieve more efficient and environmentally friendly $BaTiO_3$ powder synthesis processes.

In this research, the initial step involved analyzing $BaTiO_3$ samples that were synthesized using the solid-state direct calcination method. Subsequently, ball treatments were applied to both the mixed raw materials and the barium titanate product. This approach aimed to investigate the impact of a two-step ball milling process on the synthesized barium titanate. Afterwards, the raw materials used for synthesis were replaced with nanoscale $BaCO_3$ and nano-TiO_2 with different particle sizes, and the influence of different particle sizes of raw materials on the synthesized barium titanate was discussed. These two methods effectively eliminated impurities that are prone to occur in solid-state synthesis and achieved a uniform and fine $BaTiO_3$ particle size.

The solid-state synthesis method involved in this study successfully synthesized $BaTiO_3$ particles with an average particle size (D50) of about 170 nm, exhibiting excellent uniformity and high tetragonality with a *c/a* near 1.01022. The synthesized barium titanate powder has important prospects for the miniaturization of electronic devices, as it maintains high tetragonality while ensuring uniform particle size.

2. Materials and Methods

2.1. Materials

Titanium dioxide (TiO_2, 5–10 nm, 99.8%) was purchased from JiuDing Biotechnology, Shanghai, China. Titanium dioxide (TiO_2, 25 nm, 99.8%) was purchased from Macklin Biochemical Technology, Shanghai, China. Titanium dioxide (TiO_2, 40 nm, 99.8%) was purchased from Aladdin Biochemical Technology, Shanghai, China. Titanium dioxide (TiO_2, 99%) was purchased from Meryer Chemical Technology, Shanghai, China. Barium carbonate ($BaCO_3$, 0.5–1.5 μm, 99.8%) was purchased from Aladdin Biochemical Technology, Shanghai, China. Barium carbonate ($BaCO_3$, 99% in 30–80 nm) was purchased from Maya Reagent. Ethanol (C_2H_5O, ≥99.8%) was bought from Macklin Biochemical Technology, Shanghai, China. All reagents were used directly after purchase.

2.2. Preparation of BaTiO₃ Particles

This solid-state synthesis method for $BaTiO_3$ involves the use of two primary raw materials, titanium dioxide (TiO_2) and barium carbonate ($BaCO_3$). This study incorporated three different particle sizes of an anatase-type TiO_2 (5–10 nm, 25 nm, and 40 nm) and two variations of $BaCO_3$ (micrometer-scale and 30–80 nm scale). The raw materials were mixed in a stoichiometric molar ratio of Ba to Ti elements (Ba: Ti = 1:1), and for the preparation of the composite, 0.6 g of TiO_2 and 2.467 g of $BaCO_3$ were blended in a

laboratory beaker. Figure 1 illustrates the detailed synthetic and fabrication process of $BaTiO_3$ employed in this research.
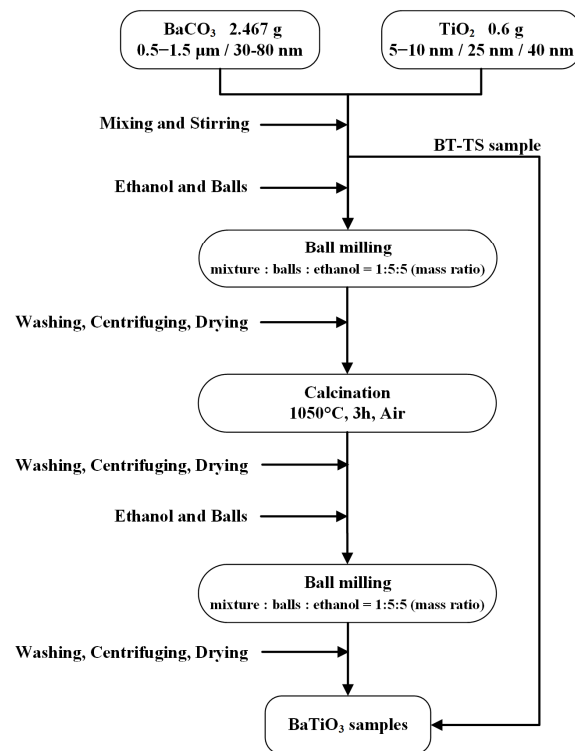

Figure 1. Flow chart for the preparation of $BaTiO_3$ samples.

The resulting amalgamation was then transferred to a 50 mL stainless steel ball milling jar, where it was processed using zirconium oxide grinding balls within an ethanol milieu. The mass ratio of raw materials to grinding balls to ethanol was set at 1:5:5, and the ball milling rotation speed was 240 rounds per minute (rpm).

After the initial ball milling pretreatment, the amalgamated mixture was transferred to alumina crucibles for the calcination process, which was conducted under ambient air conditions at a temperature of 1050 °C for 3 h. Following calcination, the raw $BaTiO_3$ product was pulverized and subjected to a second ball milling, employing identical parameters as in the prior operation. The solid–liquid mixture was then transferred into a centrifuge tube and subjected to a single centrifugation cycle. The resulting product was subjected to successive rinses and an acetic acid solution. Following the decantation of the supernatant, the residual material was desiccated in an oven set to 80 °C for 12 h. Finally, the resulting desiccated white $BaTiO_3$ solid was comminuted into a finely powdered form.

2.3. Characterization of $BaTiO_3$ Particles

The crystal phase and lattice constants of $BaTiO_3$ particles were analyzed using X-ray diffraction instrument (XRD, D8 Advanced, Bruker AXS GmbH, Karlsruhe, Germany) with Cu K_α radiation at 40 kV and 40 mA. The morphology of $BaTiO_3$ was analyzed using a scanning electron microscope (SEM, Hitachi S4800, Tokyo, Japan). The particle size distribution and average particle sizes (D50) of the $BaTiO_3$ powders were determined using a particle size analyzer (Mastersizer 2000, Malvern Instruments Ltd., Worcestershire, UK). The measurement range spanned from 0.02 μm to 2000 μm, and the ethanol was used as the dispersant. The element distribution was analyzed using energy dispersive spectrometer (EDS) equipment (Ultim Max, Oxford Instruments, Oxford, UK) and X-ray photoelectron spectroscopy (XPS) equipment (K-Alpha, Thermo Scientific, Waltham, MA, USA).

3. Results and Discussion

3.1. Analysis of Barium Titanate Synthesized by Direct Calcination

Figure 2 displays the X-ray diffraction pattern of the $BaTiO_3$ sample (BT-TS), synthesized via the traditional solid-state synthesis method, which involved calcining a mixture of micrometer-scale $BaCO_3$ and TiO_2 precursors at 1050 °C and 3 h under an air atmosphere. In Figure 2, the main diffraction peaks aligned with the tetragonal *P4mm* space group characteristic of $BaTiO_3$ (JCPDS 74-1957), confirming that $BaTiO_3$ has been synthesized. However, upon the comparative analysis with the standard PDF card, impurities were identified, including $BaTi_4O_9$ (JCPDS 34-0070), unreacted TiO_2 (JCPDS 07-4874), and $BaCO_3$ (JCPDS 45-1471) raw materials.
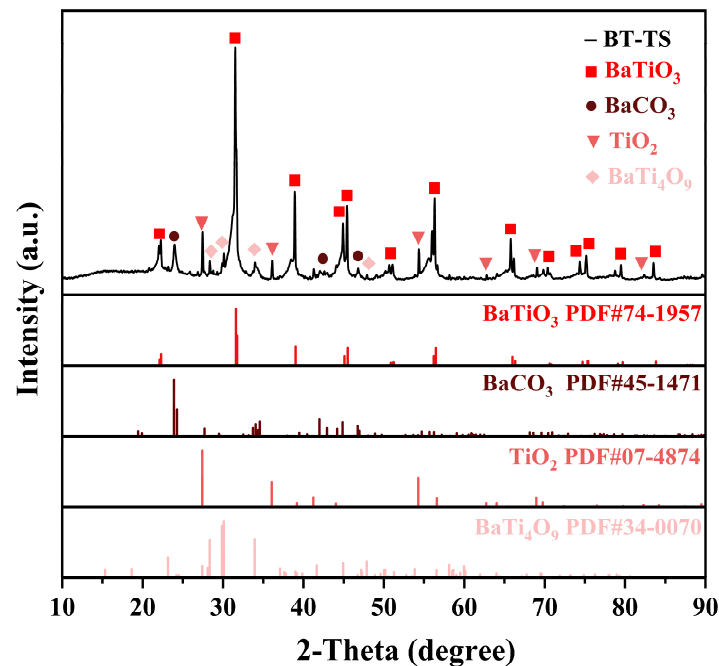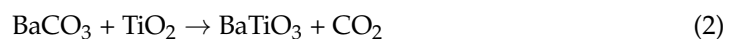

Figure 2. XRD pattern of $BaTiO_3$ sample BT-TS.

In solid-state reactions, the intermediate processes of barium titanate synthesis can be summarized as follows [18]. The first step is to directly decompose the $BaCO_3$ raw material powder into BaO and CO_2 gas in a high-temperature reaction. Part of $BaCO_3$ reacts with the titanium source TiO_2 to generate the product $BaTiO_3$, while the remaining $BaCO_3$ generates the Ba_2TiO_4 phase, which is expressed as the following reaction:

$$BaCO_3 \rightarrow BaO + CO_2 \tag{1}$$

$$BaCO_3 + TiO_2 \rightarrow BaTiO_3 + CO_2 \tag{2}$$

$$2BaCO_3 + TiO_2 \rightarrow Ba_2TiO_4 + 2CO_2 \tag{3}$$

In this step, the Gibbs free energy of $BaCO_3$ decomposition is the lowest, making it the main reaction in this part. In the second step, the BaO generated by the first reaction will simultaneously generate the Ba_2TiO_4 phase, which can be expressed as

$$BaO + TiO_2 \rightarrow BaTiO_3 \tag{4}$$

$$2BaO + TiO_2 \rightarrow Ba_2TiO_4 \tag{5}$$

This indicates that there will be products generated by the non-1:1 combination of Ba and Ti during the calcination process. It also explains the impurities in Figure 2, which are the remaining raw materials that have not fully reacted and the source of $BaTi_4O_9$

generated due to an insufficient reaction. In order to eliminate impurities and synthesize pure barium titanate powder to solve the impurity problem in the solid-state method, the next section of research on the ball milling treatment is introduced from the perspective of the binding and mixing of raw materials before calcination.

3.2. The Effect of Ball Milling Treatment on the Synthesized Barium Titanate

In order to investigate the effects of two-step ball milling on the synthesis process, four different samples were synthesized. The four different samples include the following:

- BT0-0 is $BaTiO_3$ sample synthesized without any ball milling treatment.
- BT0-1 is $BaTiO_3$ sample synthesized solely for ball milling of raw $BaTiO_3$.
- BT1-0 is $BaTiO_3$ sample synthesized solely for ball milling of raw materials.
- BT1-1 is $BaTiO_3$ sample synthesized by both two-step ball milling treatment.

The raw materials for these four samples are TiO_2 and micrometer-sized $BaCO_3$, and the calcination conditions are all 1050 °C and 3 h. The mass ratio of raw materials to grinding balls to ethanol was set at 1:5:5, and the ball milling process had a rotation speed of 240 rpm. The XRD patterns of the four $BaTiO_3$ samples synthesized with and without ball milling are shown in Figure 3. Firstly, for the samples BT0-0 and BT0-1, the XRD patterns clearly show not only the characteristic peaks of the tetragonal *P4mm* space group $BaTiO_3$ (JCPDS 74-1957) that was mainly synthesized but also a significant number of peaks corresponding to impurities. Similar to BT-TS, these two samples were not subjected to ball milling of the raw materials. Comparing BT0-0 with BT1-0, it is not difficult to find that after ball milling of the raw materials followed by synthesis, the characteristic peaks of the tetragonal *P4mm* space group $BaTiO_3$ (JCPDS 74-1957) in the XRD pattern of BT1-0 are very distinct and basically consistent with the PDF standard cards. This indicates that ball milling of the raw materials indeed promotes the synthesis reaction and makes the reaction more complete, with impurities essentially disappearing. However, it is still possible to observe minor impurity peaks in the range of $2\theta = 25°-30°$, which is noteworthy. Lastly, for the sample BT1-1, the standard PDF card comparison result is essentially consistent with that of BT1-0, and there are still minor impurity peaks in the range of $2\theta = 25°-30°$, indicating that the simple introduction of ball milling cannot completely eliminate the impurity issues in solid-state synthesis methods, and further analysis and research from other perspectives are necessary.
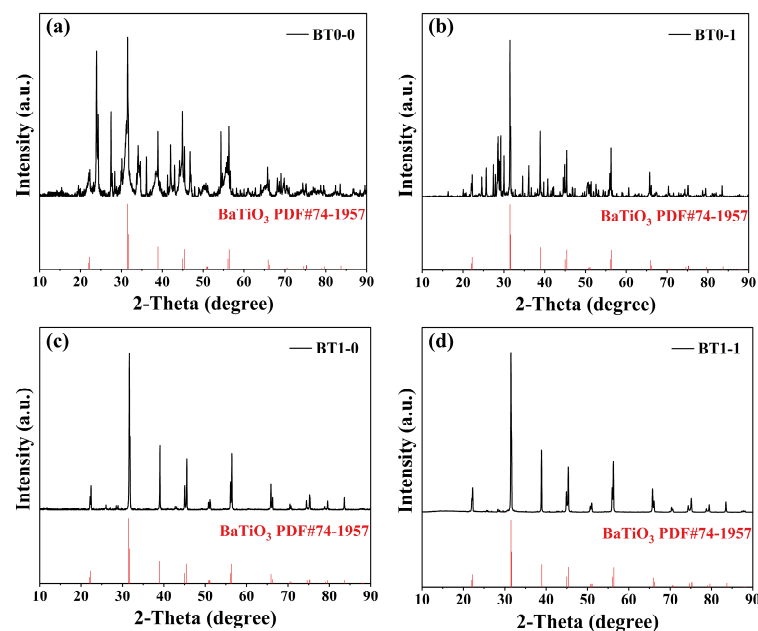

Figure 3. Main XRD patterns of $BaTiO_3$ samples synthesized with and without ball milling: (**a**) BT0-0, (**b**) BT0-1, (**c**) BT1-0, and (**d**) BT1-1.

On the other hand, the impact of the introduction of ball milling on the tetragonality of the synthesized $BaTiO_3$ is also very much worth noting. Therefore, based on the analysis and calculation of the crystal structures of the four samples in the software JADE 9.0, different tetragonalities c/a were obtained, as shown in Table 1. From Table 1, it can be seen that the tetragonality of the samples is all around 1.01 except BT0-1, which on one hand indicates that the tetragonality of $BaTiO_3$ synthesized by the solid-state method is indeed good. The tetragonality is affected due to the fact that BT0-0 and BT0-1 did not produce pure $BaTiO_3$. On the other hand, by comparing the tetragonality of BT1-0 and BT1-1, it can be seen that ball milling of the $BaTiO_3$ has no negative impact on the tetragonality.

Table 1. *c/a* and distributions of particle sizes.

Sample	*c/a*	D_{10} (μm)	D_{50} (μm)	D_{90} (μm)
BT0-0	1.01138	0.965	6.125	20.179
BT0-1	1.00586	0.648	3.551	15.214
BT1-0	1.01049	0.134	0.182	2.620
BT1-1	1.01017	0.131	0.171	0.226

Figure 4 presents the SEM micrographs of the aforementioned four samples. Firstly, from a cross-sectional comparison perspective, it is observed that the samples BT0-0 and BT0-1 share some common morphological characteristics. Specifically, fine particles can be observed adhering to larger particles in both samples. However, the agglomeration of particles in the BT0-1 sample is significantly reduced, indicating that the ball milling of $BaTiO_3$ has improved the interparticle interactions and enhanced the dispersion of the particles.
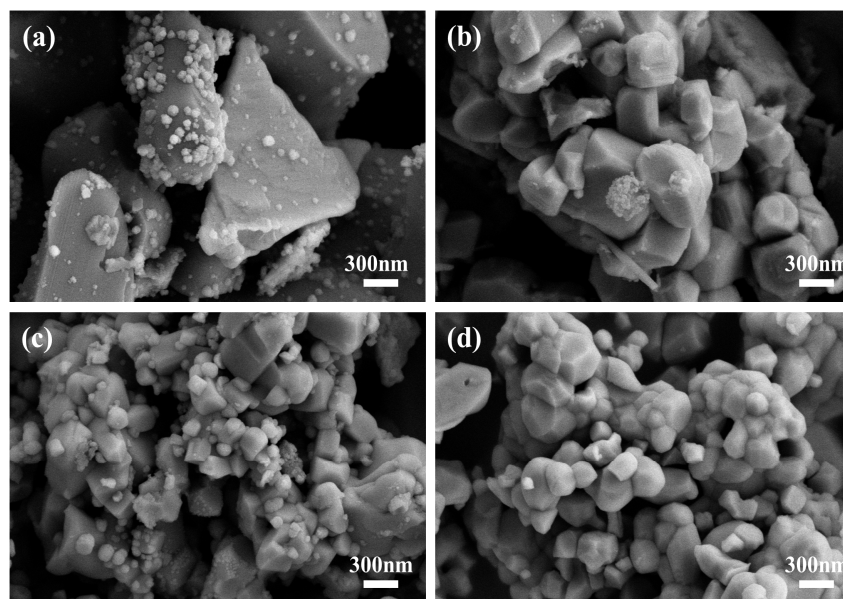

Figure 4. SEM images of $BaTiO_3$ samples synthesized with and without ball milling: (**a**) BT0-0, (**b**) BT0-1, (**c**) BT1-0, and (**d**) BT1-1.

Secondly, through a longitudinal comparison, it can be noted that the samples BT1-0 and BT1-1, in contrast to the samples BT0-0 and BT0-1, no longer exhibit the phenomenon of fine particles adhering to larger particles. This change may be due to the ball milling process, which allows for a more thorough mixing of the raw materials, leading to an increase in the surface energy, Gibbs free energy, and activation energy of the crystals. Consequently, in the subsequent synthesis reaction, the interactions between the raw materials are more complete, and the reaction process is more thorough and in-depth.

When the cumulative particle size distribution percentage reaches 10%, 50%, and 90%, the sample particle sizes are represented as D10, D50, and D90, respectively, indicating that particles smaller than these values account for 10%, 50%, and 90%. These three values provide a relatively intuitive view of the particle size distribution of the powder [19]. D10 and D90 represent the fine and coarse diameters of the powder, respectively, while D50 is the median particle size of the powder. The particle size distribution and average particle sizes (D50) of the $BaTiO_3$ powders were determined using a particle size analyzer (Mastersizer 2000, Malvern Instruments Ltd., Worcestershire, UK).

The D10, D50, and D90 data recorded in Table 1 provide us with a quantitative perspective to evaluate the impact of ball milling on the particle size distribution of $BaTiO_3$ titanate samples. These data represent the particle sizes corresponding to 10%, 50%, and 90% of the particles in the sample, which are important parameters for describing the characteristics of the particle size distribution.

For the two samples, BT0-0 and BT0-1, it can be observed that the BT0-1 sample, which underwent ball milling of $BaTiO_3$, has reduced values in all three parameters of D10, D50, and D90. Specifically, the average particle size (D50) of BT0-1 decreased from 6.125 μm to 3.551 μm, and the D10 and D90 values also decreased accordingly, indicating that the overall particle size of the sample was significantly reduced after ball milling. This result is consistent with the morphological changes observed by SEM; that is, ball milling can effectively reduce particle size and improve particle dispersion.

More notably, the particle size distribution data of the BT1-1 sample is significant. The average particle size of the BT1-1 sample is 0.171 μm, and its particle size distribution is very concentrated, with most particles ranging from 0.131 μm to 0.226 μm in size. This result indicates that the BT1-1 sample, after the second ball milling process, not only has an extremely small particle size but also a highly uniform particle size distribution. This demonstrates that ball milling plays a key role in controlling the particle size distribution of barium titanate powder, especially in achieving a highly uniform distribution.

In summary, the D10, D50, and D90 data presented in Table 1 allow for a quantitative analysis and comparison of the effects of different ball milling treatments on the particle size distribution of $BaTiO_3$ samples. These data, combined with SEM observations, provide us with a comprehensive perspective to understand the specific effects of ball milling on the morphology and particle size distribution of $BaTiO_3$ samples. These analyses lead to the conclusion that ball milling is an effective method for optimizing the particle size distribution of barium titanate powder, potentially enhancing its final performance.

The ball milling treatment had a significant positive effect on improving the morphology and particle size distribution of barium titanate samples. In particular, after ball milling of $BaTiO_3$, the particle size distribution of the barium titanate samples was significantly optimized. The particle sizes became more uniform and concentrated. Compared with the samples that were not subjected to ball milling, there was a noticeable reduction in the average particle size, which was clearly demonstrated in both the SEM images and the particle size distribution data. The decrease in parameters such as D10, D50, and D90 further confirmed the effectiveness of the ball milling treatment.

3.3. The Influence of Raw Materials with Different Particle Sizes on the Synthesis of Barium Titanate

In this part, the $BaTiO_3$ samples were synthesized using micrometer-sized (BC-μm) and 30−80 nm sized $BaCO_3$ (BC-nm). The calcination conditions are all 1050 °C and 3 h. The mass ratio of raw materials to grinding balls to ethanol was set at 1:5:5, and the ball milling process had a rotation speed of 240 rpm.

Figure 5 presents the XRD pattern of BC-μm and BC-nm. For both BC-μm and BC-nm samples, the XRD results indicate that the main diffraction peaks correspond to the characteristics of the tetragonal *P4mm* space group of $BaTiO_3$ (JCPDS 74-1957), once again confirming the successful synthesis of $BaTiO_3$. Compared to the BT-TS sample in Figure 2, the absence of peaks for unreacted TiO_2 and $BaCO_3$ is very evident, indicating that the

ball milling process can effectively promote a comprehensive reaction of the raw materials, thereby significantly reducing the presence of unreacted raw materials. Moreover, the peaks for $BaTi_4O_9$ have also completely disappeared, further demonstrating the significant effect of the ball milling process in improving reaction efficiency and reducing impurities.
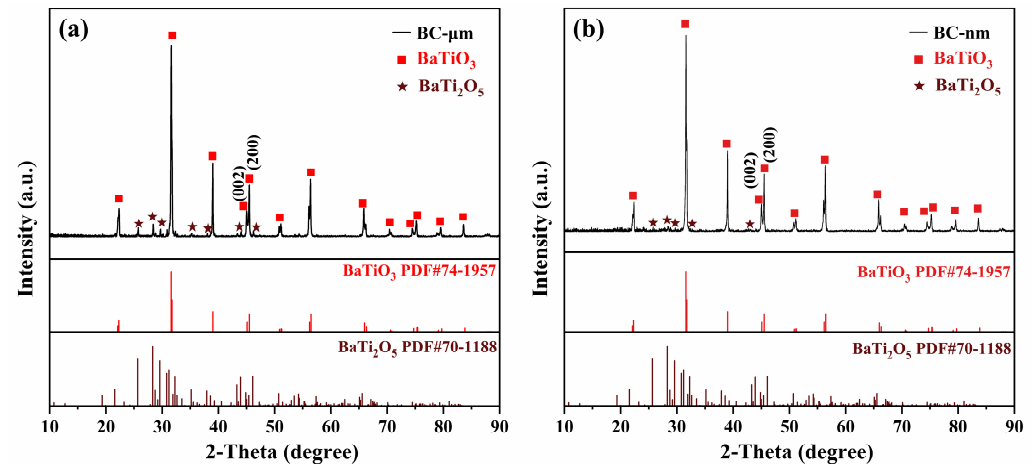

Figure 5. XRD patterns of $BaTiO_3$ samples synthesized by $BaCO_3$ with different particle sizes: (**a**) BC-μm and (**b**) BC-nm.

Despite undergoing two stages of ball milling treatment, minor impurities are still observable in the XRD results of both BC-μm and BC-nm near 25° and 28°. By comparing with the standard PDF cards, these peaks are identified as $BaTi_2O_5$ (JCPDS 70-1188). Compared to the $BaTi_4O_9$ present in BT-TS, where the ratio of Ba to Ti elements is 1:4, $BaTi_2O_5$ exhibits a higher ratio of 1:2, indicating a higher degree of reaction between Ba and Ti elements. Although the BC-μm and BC-nm samples have improved in terms of impurities and element ratios compared to the BT-TS sample, it is noteworthy that the element ratio of Ba to Ti has not yet reached the ideal 1:1 ratio. This suggests that the micro-level interaction between Ba and Ti still needs to be enhanced, and therefore the BC-μm and BT40 samples are not entirely composed of pure $BaTiO_3$. This finding suggests that while the ball milling treatment played a positive role in reducing impurities during the calcination process, completely eliminating the presence of impurities remains a challenge.

In the XRD results of BC-μm and BC-nm, the split peaks near $2\theta = 45°$ for the (002) and (200) crystal planes provide key evidence for the successful synthesis of the tetragonal phase of $BaTiO_3$. The symmetrical shape and non-split state of these peaks further confirm the tetragonal structure of the BC-μm and BC-nm samples. Crystallographic calculations using the JADE software show a *c/a* ratio of 1.00964 for the BC-μm sample and a ratio of 1.00986 for the BC-nm sample. On the other hand, it also suggests that the use of nano-sized $BaCO_3$ rarely has an impact on the tetragonality of the synthesized barium titanate.

Generally, TiO_2 with a smaller particle size, due to its larger specific surface area, reacts more rapidly with $BaCO_3$, which helps to improve the efficiency of barium titanate synthesis. The particle size of titanium dioxide may affect the final crystal structure of barium titanate. The particle size distribution of titanium dioxide has a direct impact on the particle size distribution of barium titanate powder. A uniform particle size of titanium dioxide is conducive to obtaining a barium titanate powder with a uniform particle size distribution, which is particularly important for the preparation of high-performance electronic ceramic materials. To thoroughly investigate and address the issue of residual $BaTi_2O_5$ impurities in the BC-μm and BC-nm samples, and to fully understand the specific effects of different TiO_2 particle sizes on the crystal structure and morphology of $BaTiO_3$, this section simultaneously uses TiO_2 with different particle sizes (5–10 nm, 25 nm, and 40 nm) to synthesize three samples, BT5-10, BT25, and BT40, based on the use of nano-sized $BaCO_3$ as the raw material. The calcination conditions are all 1050 °C and 3 h.

The mass ratio of raw materials to grinding balls to ethanol was set at 1:5:5, and the ball milling process had a rotation speed of 240 rpm.

Figure 6, from top to bottom, shows the XRD and the locally enlarged XRD diagrams of the three samples. In Figure 6a, the XRD results of all three samples are consistent with the standard PDF card (JCPDS 74-1957), confirming that the synthesized crystals are $BaTiO_3$. This result indicates that nano-sized raw materials with different particle sizes can effectively be used to produce $BaTiO_3$ with a stable structure. Compared with BT40, no impurity peaks were observed in the XRD diagram of BT5-10, confirming that the introduction of ball milling technology and the use of nano-sized raw materials can effectively eliminate impurities such as $BaTi_4O_9$ and $BaTi_2O_5$. The results in Figure 6b further reveal that all three samples have split peaks near $2\theta = 45°$ for the (002) and (200) crystal planes, which provides key evidence for the successful synthesis of the tetragonal phase of $BaTiO_3$. In Figure 6b, the red curve represents the fitting of the split peaks at 45° for different samples. The symmetrical shape and non-split state of these peaks further confirm the existence of the tetragonal structure. It is noteworthy that the splitting between these two peaks is most pronounced in the BT5-10 sample, indicating that it has the best tetragonality.
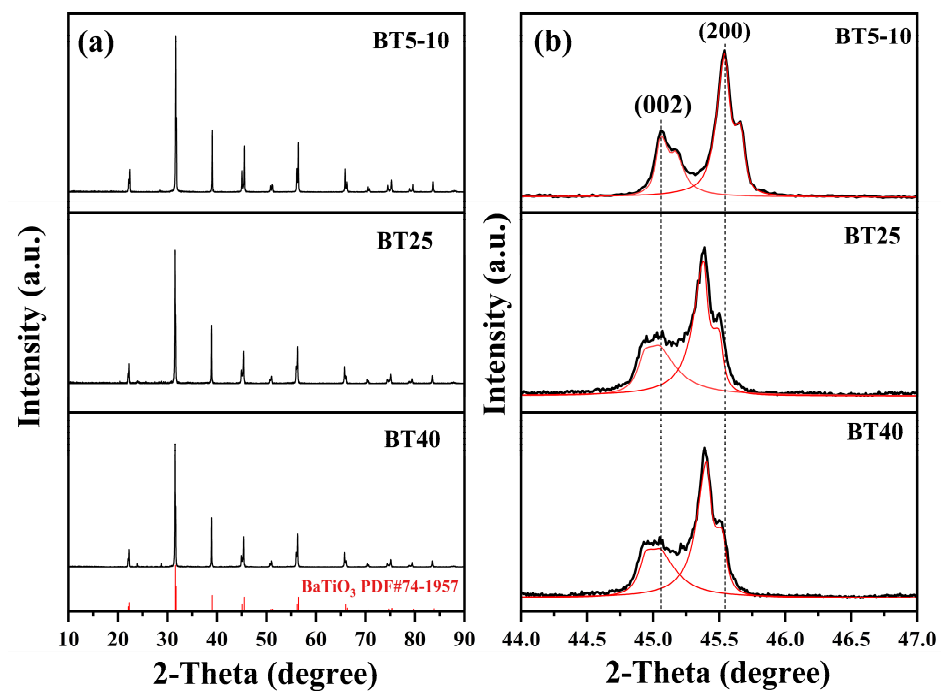

Figure 6. XRD patterns of $BaTiO_3$ samples synthesized using different sizes of TiO_2 precursors: (**a**) XRD patterns of BT5-10, BT25, and BT40; (**b**) XRD patterns of BT5-10, BT25, and BT40 after amplification.

Figure 7 presents the SEM images of the three samples, providing intuitive information about the sample morphology. As shown in Figure 7a, the BT5-10 sample exhibits the best particle dispersion and distribution among all the samples. This may be attributed to the smaller particle size of TiO_2, which provides a larger specific surface area and higher reactivity, thus promoting more uniform mixing and dispersion. The BT25 sample in Figure 7b, while also showing improved particle dispersion, has slightly less uniformity compared to BT5-10. In contrast, the BT40 sample in Figure 7c displays a noticeable particle agglomeration and poorer dispersion.
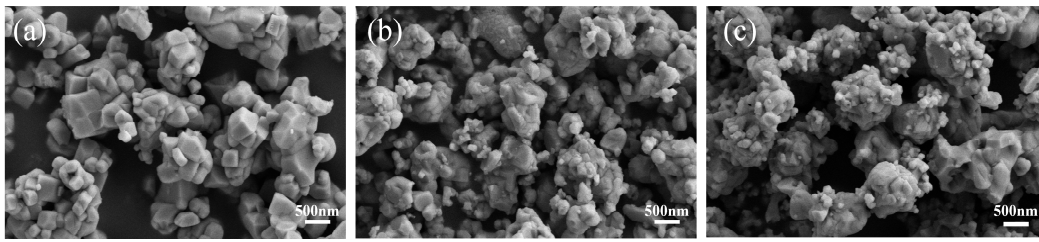
Figure 7. SEM images of BT5-10, BT25, and BT40: (**a**) SEM image of BT5-10; (**b**) SEM image of BT25; (**c**) SEM image of BT40.

According to the data presented in Table 2, the *c/a* ratios for the three samples are 1.01022, 1.00941, and 1.00924, respectively. From these data, it is evident that the BT5-10 sample exhibits the best tetragonality. This result further confirms that the use of nano-sized raw materials has a significant impact on enhancing the tetragonal nature of $BaTiO_3$. Due to their higher specific surface area and reactivity, nano-sized raw materials can provide a more uniform and refined reaction environment during the synthesis process, which is conducive to forming a more complete crystal structure and improving the tetragonality of $BaTiO_3$.

Table 2. *c/a* and distributions of particle sizes.

Sample	*c/a*	D10 (μm)	D50 (μm)	D90 (μm)
BT5-10	1.01022	0.129	0.170	0.224
BT25	1.00941	0.132	0.177	0.253
BT40	1.00924	0.134	0.174	0.232

Furthermore, the study also found that, with the condition that $BaCO_3$ is nano-sized, and other synthesis parameters remain unchanged after the two-step ball milling treatment, the smaller the particle size of nano-TiO_2, the better the tetragonal nature of the synthesized $BaTiO_3$. This may be because the smaller particle size of TiO_2 is beneficial for improving the homogeneity of the raw material mixture, reducing particle agglomeration, and thus forming more uniform and well crystallographically oriented barium titanate particles during the sintering process. $BaTiO_3$ tends to form on the surface of TiO_2 particles. When a surface layer of $BaTiO_3$ is formed, the kinetics are controlled by the diffusion of barium and oxygen ions through this layer into the original TiO_2 phase. Since these ions are in excess on the surface layer, the Ba_2TiO_4 phase is typically formed initially.

Due to continuous diffusion, the interaction of Ba_2TiO_4 and TiO_2 gradually formed uniform $BaTiO_3$ particles. It suggests that fine anatase TiO_2 with a low density and a large surface area enhances the formation of $BaTiO_3$ by reducing the activation energy, which is consistent with our findings.

Table 2 also lists the D10, D50, and D90 values for the three samples. It is observed that the average particle size of all three samples is around 170 nm.

Due to the fact that sample BT5-10 not only ensures a high degree of tetragonality (1.01022) but also maintains a relatively small particle size (170 nm), specific elemental composition analysis was conducted on this sample to verify the purity of barium titanate and ensure uniform elemental distribution.

The energy-dispersive spectroscopy (EDS) data and quantitative elemental analysis for BT5-10 are presented in Figure 8. The sample exhibits an atomic composition of Ba (18.95%), Ti (19.01%), and O (61.18%), which approximates the 1:1:3 ratio characteristic of the stoichiometry of $BaTiO_3$ [20].

X-ray photoelectron spectroscopy (XPS) was conducted on the BT5-10 sample to achieve a more nuanced understanding of its elemental composition. The XPS results of BT5-10 are shown in Figure 9.
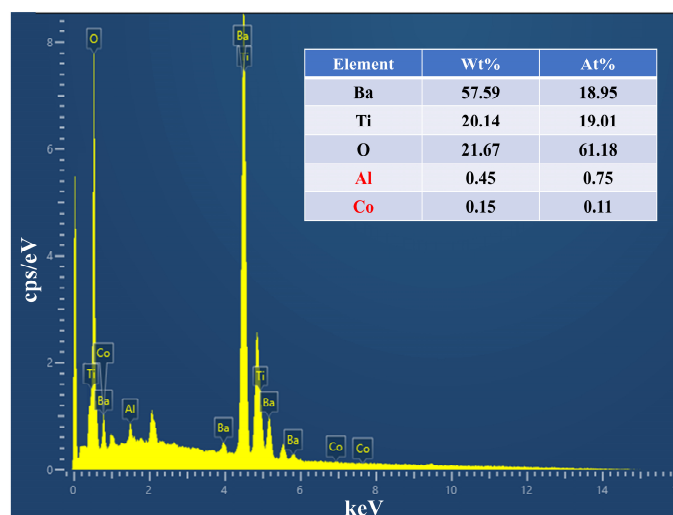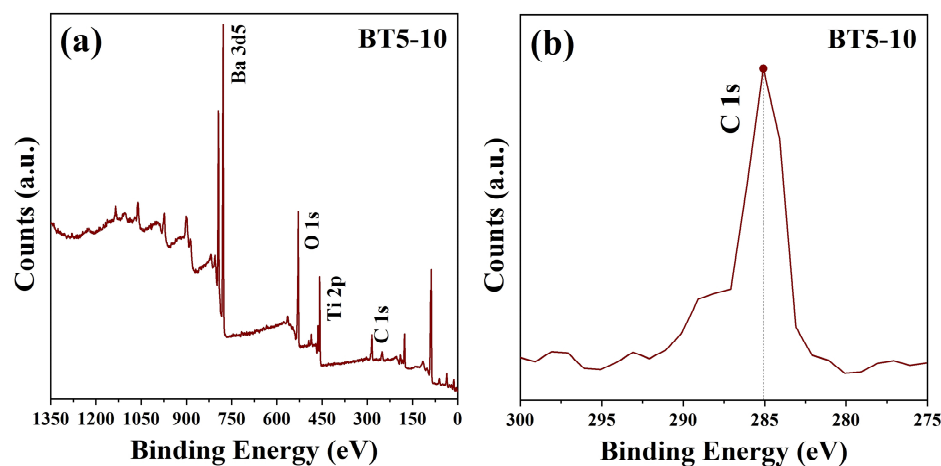
Figure 8. EDS images of BT5-10.

Figure 9. XPS images of BT5-10: (**a**) full spectra XPS of BT5-10; (**b**) High resolution XPS spectra of C 2*p*.

Figure 9a illustrates the high-resolution XPS spectrum of BT5-10. The distinct peaks observed at binding energies between 700 and 800 eV are assigned to the Ba $3d_{5/2}$ and Ba $3d_{3/2}$ levels, indicative of the perovskite structure characteristic of BaTiO₃ [21].

The peaks in the vicinity of 450 eV are associated with the Ti $2p_{3/2}$ and Ti $2p_{1/2}$ transitions, which are diagnostic of the Ti⁴⁺ oxidation state. The absence of a lower binding energy satellite peak associated with the Ti $2p_{3/2}$ signifies that titanium ions are exclusively present in the oxidation state. This observation further supports the tetragonal structure of the material and indicates the absence of Ti vacancy defects in the synthesized samples [21].

Figure 9b displays the carbon peak C 1*s* from the XPS results of the BT5-10 sample. It is evident that the carbon peak is distributed very close to 285 eV, indicating that the sample does not contain impurity carbon but rather suggests the presence of adventitious carbon, likely introduced during the testing process as amorphous organic carbon [22].

Table 3 presents a comparison of particle size and tetragonality of barium titanate samples synthesized by different synthetic methods.

Based on a comprehensive analysis of the experimental data presented in this paper, it can be concluded that, provided that BaCO₃ is nano-sized, the particle size of nano-TiO₂ has a significant impact on the tetragonal nature of the synthesized BaTiO₃ through a two-step ball milling process, with other synthesis parameters remaining constant. Specifically, using nano-TiO₂ with a smaller particle size as the raw material can more effectively

promote the formation of the tetragonal phase of $BaTiO_3$, thereby enhancing the material's tetragonal nature.

Table 3. Research results of synthesized $BaTiO_3$.

Researchers	Heat Treatment (°C)	Particle Size (nm)	Tetragonality (*c/a*)	Method
Maison et al. [23]	1100	392	1.0098	Catecholate process
Kown et al. [24]	1000	243	1.0074	Hydrothermal
	1000	326	1.0105	
Tihtih et al. [25]	800	26.15	1.0021	Sol–gel process
	900	29.65	1.0054	
	1000	32.46	1.0063	
Clabel et al. [26]	1000	240	1.0060	Solid-state reaction
	1100	360	1.0081	
Xiaoxiao Pang et al. [27]	-	82	1.0088	Hydrothermal
Tingting Wang et al. [28]	-	near 160	near 1.00895	Hydrothermal
This work	1050	170	1.01022	Solid-state reaction

In this study, the BT5-10 sample synthesized using 5–10 nm TiO_2 as the raw material demonstrated the best particle dispersion and distribution among all the compared samples, with an average particle size of 170 nm and a tetragonal nature of 1.01022.

4. Conclusions

In this study, a novel solid-state synthesis method was employed to prepare barium titanate ($BaTiO_3$) powder, which is characterized by its high tetragonal nature, small particle size, and uniform distribution. The novel synthesis method primarily involves the use of small-sized raw materials and the ball milling treatment for both the raw materials and the coarse products.

Comprehensive characterizations, including XRD, SEM, LDM, EDS, and XPS, were conducted to evaluate the synthesized $BaTiO_3$ powder, leading to the following conclusions:

(1) Ball milling treatment does not have a negative impact on the tetragonality. It resulted in a more homogeneous mixture of the raw materials, which helped to prevent the appearance of impurities after sintering.

(2) Ball milling treatment has a significant positive effect on improving the morphology and particle size distribution of $BaTiO_3$.

(3) The replacement with nano-sized $BaCO_3$ did not significantly affect the tetragonality or improve the particle size distribution and morphology of the synthesized $BaTiO_3$.

(4) The particle size of nano-TiO_2 has a significant impact on the tetragonality of $BaTiO_3$. Generally, using smaller-sized nano-TiO_2 as a raw material can more effectively promote the formation of the tetragonal phase of $BaTiO_3$.

In this study, the BT5-10 sample synthesized using 5–10 nm TiO_2 as the raw material showed the best particle dispersion and distribution among all the compared samples, with an average particle size of 170 nm and a tetragonal nature of 1.01022. This meets the contemporary electronic industry's demand for high tetragonal nature, small, and uniformly sized $BaTiO_3$ particles and also addresses some of the issues present in the solid-state method.

Author Contributions: Data curation, T.H. and J.S.; Funding acquisition, J.S.; Investigation, T.H., J.S. and Q.P.; Methodology, T.H., J.S., Q.P. and C.Z.; Project administration, J.S., J.L. and C.Z.; Resources, W.H. and C.Z.; Supervision, J.S., J.L., W.H. and C.Z.; Visualization, T.H.; Writing—original draft, T.H.; Writing—review and editing, T.H., J.L. and C.Z. All authors have read and agreed to the published version of the manuscript.

Institutional Review Board Statement: Not applicable.

Informed Consent Statement: Not applicable.

Data Availability Statement: Data are contained within the article.

Conflicts of Interest: Author Jing Shen was employed by the company Chongqing Newcent New Materials Co., Ltd. The remaining authors declare that the research was conducted in the absence of any commercial or financial relationships that could be construed as a potential conflict of interest.

References

1. Humera, N.; Arshad, F.; Raza, A.; Raza, M.A.; Atiq, S.; Kayani, Z.N.; Naseem, S.; Riaz, S. Dielectric and ferroelectric properties of X8R perovskite barium titanate for application in multilayered ceramics capacitors. *J. Mater. Sci. Mater. Electron.* **2022**, *33*, 7405–7422. [CrossRef]
2. Sebastian, T.; Michalek, A.; Hedayati, M.; Lusiola, T.; Clemens, F. Enhancing dielectric properties of barium titanate macrofibers. *J. Eur. Ceram. Soc.* **2019**, *39*, 3716–3721. [CrossRef]
3. Li, R.; Wei, W.; Hai, J.; Gao, L.; Gao, Z.; Fan, Y. Preparation and electric-field response of novel tetragonal barium titanate. *J. Alloys Compd.* **2013**, *574*, 212–216. [CrossRef]
4. Hoshina, T. Size effect of barium titanate: Fine particles and ceramics. *J. Ceram. Soc. Jpn.* **2013**, *121*, 156–161. [CrossRef]
5. Jiang, B.; Iocozzia, J.; Zhao, L.; Zhang, H.; Harn, Y.W.; Chen, Y.; Lin, Z. Barium titanate at the nanoscale: Controlled synthesis and dielectric and ferroelectric properties. *Chem. Soc. Rev.* **2019**, *48*, 1194–1228. [CrossRef]
6. Lv, L.; Wang, Y.; Gan, L.; Liu, Q.; Zhou, J.-P. Sintering process effect on the BaTiO$_3$ ceramic properties with the hydrothermally prepared powders. *J. Mater. Sci. Mater. Electron.* **2018**, *29*, 14883–14889. [CrossRef]
7. Li, Z.; Yan, S.; Xia, J.; Cao, F.; Chen, X.; Song, Y.; Chen, Y.; Lin, Z.-S.; Wang, G. Direct current (dc) bias effect on the dielectric constant of Dy and Ho-doped BaTiO$_3$-based ceramic and MLCCs. *Ceram. Int.* **2022**, *48*, 27439–27447. [CrossRef]
8. Zhu, C.; Cai, Z.; Feng, P.; Zhang, W.; Hui, K.; Cao, X.; Fu, Z.; Wang, X. Reliability Mechanisms of the Ultrathin-Layered BaTiO$_3$-Based BME MLCC. *Acta Phys. Chim. Sin.* **2023**, *40*, 2304015. [CrossRef]
9. Uchino, K.; Sadanaga, E.; Hirose, T. Dependence of the Crystal Structure on Particle Size in Barium Titanate. *J. Am. Ceram. Soc.* **2005**, *72*, 1555–1558. [CrossRef]
10. Kutty, T.R.N.; Vivekanandan, R.; Murugaraj, P. Precipitation of rutile and anatase (TiO$_2$) fine powders and their conversion to MTiO$_3$ (M= Ba, Sr, Ca) by the hydrothermal method. *Mater. Chem. Phys.* **1988**, *19*, 533–546. [CrossRef]
11. Kita, T.; Kondo, S.; Takei, T.; Kumada, N.; Nakashima, K.; Fujii, I.; Wada, S.; Suzuki, T.S.; Uchikoshi, T.; Sakka, Y.; et al. Preparation and characterization of Grain-Oriented Barium Titanate Ceramics Using Electrophoresis Deposition Method under A High Magnetic Field. *IOP Conf. Ser. Mater. Sci. Eng.* **2011**, *18*, 092041. [CrossRef]
12. Wada, S.; Narahara, M.; Hoshina, T.; Kakemoto, H.; Tsurumi, T. Preparation of nm-sized BaTiO$_3$ particles using a new 2-step thermal decomposition of barium titanyl oxalate. *J. Mater. Sci.* **2003**, *38*, 2655–2660. [CrossRef]
13. On, D.V.; Vuong, L.D.; Chuong, T.V.; Quang, D.A.; Tung, V.T. Study on the synthesis and application of BaTiO$_3$ nanospheres. *Int. J. Mater. Res.* **2021**, *112*, 448–456. [CrossRef]
14. Gromada, M.; Biglar, M.; Trzepieciński, T.; Stachowicz, F. Characterization of BaTiO$_3$ piezoelectric perovskite material for multilayer actuators. *Bull. Mater. Sci.* **2017**, *40*, 759–771. [CrossRef]
15. Hao, Y.A.; Wang, X.H.; Zhang, H.; Shen, Z.B.; Li, L.T. Investigation on the synthesis procedure of ultrafine monodispersed BaTiO$_3$ powders by solvothermal method. *J. Ceram. Soc. Jpn.* **2013**, *121*, 506–511. [CrossRef]
16. Wan, L.; Zhu, G.; Xu, H.; Zhao, Y.; Cheng, Y.; Fu, Z.; Hu, C.; Yu, A. Low-temperature solid-state synthesis of tetragonal BaTiO$_3$ powders from Ba(OH)$_2$ and H$_2$TiO$_3$. *Appl. Phys. A* **2022**, *128*, 858. [CrossRef]
17. Walton, R.I.; Millange, F.; Smith, R.I.; Hansen, T.C.; O'Hare, D. Real time observation of the hydrothermal crystallization of barium titanate using in situ neutron powder diffraction. *J. Am. Chem. Soc.* **2001**, *123*, 12547–12555. [CrossRef]
18. Kainth, S.; Choudhary, R.; Upadhyay, S.; Bajaj, P.; Sharma, P.; Brar, L.K.; Pandey, O.P. Non-isothermal solid-state synthesis kinetics of the tetragonal barium titanate. *J. Solid State Chem.* **2022**, *312*, 123275. [CrossRef]
19. Mao, Y.; Gerrow, A.; Ray, E.; Perez, N.D.; Edler, K.; Wolf, B.; Binner, E. Lignin recovery from cocoa bean shell using microwave-assisted extraction and deep eutectic solvents. *Bioresour. Technol.* **2023**, *372*, 128680. [CrossRef]
20. Choi, I.; Lee, S.-J.; Kim, J.C.; Kim, Y.-g.; Hyeon, D.Y.; Hong, K.-S.; Suh, J.; Shin, D.; Jeong, H.Y.; Park, K.-I. Piezoelectricity of picosecond laser-synthesized perovskite BaTiO$_3$ nanoparticles. *Appl. Surf. Sci.* **2020**, *511*, 145614. [CrossRef]
21. Küçük, Ö.; Teber, S.; Cihan Kaya, İ.; Akyıldız, H.; Kalem, V. Photocatalytic activity and dielectric properties of hydrothermally derived tetragonal BaTiO$_3$ nanoparticles using TiO$_2$ nanofibers. *J. Alloys Compd.* **2018**, *765*, 82–91. [CrossRef]
22. Jin, M.H.; Shin, E.; Jin, S.; Jo, H.; Ok, K.M.; Hong, J.; Jun, B.-H.; Durrant, J.R. Solvothermal Synthesis of Ferroelectric BaTiO$_3$ Nanoparticles and Their Application to Dye-sensitized Solar Cells. *J. Korean Phys. Soc.* **2018**, *73*, 627–631. [CrossRef]
23. Maison, W.; Kleeberg, R.; Heimann, R.B.; Phanichphant, S. Phase content, tetragonality, and crystallite size of nanoscaled barium titanate synthesized by the catecholate process: Effect of calcination temperature. *J. Eur. Ceram. Soc.* **2003**, *23*, 127–132. [CrossRef]
24. Kwon, S.-W.; Yoon, D.-H. Tetragonality of nano-sized barium titanate powder prepared with growth inhibitors upon heat treatment. *J. Eur. Ceram. Soc.* **2007**, *27*, 247–252. [CrossRef]

25. Tihtih, M.; Ponaryadov, A.V.; Ibrahim, J.E.F.M.; Kurovics, E.; Kotova, E.L.; Gömze, L.A. Elect of temperature on the structural properties of barium titanate nanopowders synthesis via sol-gel process. *Epa. -J. Silic. Based Compos. Mater.* **2020**, *72*, 165–168. [CrossRef]

26. Clabel H, J.L.; Awan, I.T.; Pinto, A.H.; Nogueira, I.C.; Bezzon, V.D.N.; Leite, E.R.; Balogh, D.T.; Mastelaro, V.R.; Ferreira, S.O.; Marega, E. Insights on the mechanism of solid state reaction between TiO_2 and $BaCO_3$ to produce $BaTiO_3$ powders: The role of calcination, milling, and mixing solvent. *Ceram. Int.* **2020**, *46*, 2987–3001. [CrossRef]

27. Pang, X.; Wang, T.; Liu, B.; Fan, X.; Liu, X.; Shen, J.; Zhong, C.; Hu, W. Effect of solvents on the morphology and structure of barium titanate synthesized by a one-step hydrothermal method. *Int. J. Miner. Metall. Mater.* **2023**, *30*, 1407–1416. [CrossRef]

28. Wang, T.; Pang, X.; Liu, B.; Liu, J.; Shen, J.; Zhong, C. A Facile and Eco-Friendly Hydrothermal Synthesis of High Tetragonal Barium Titanate with Uniform and Controllable Particle Size. *Materials* **2023**, *16*, 4191. [CrossRef]